Atmos. Chem. Phys. Discuss., 3, 1415–1451, 2003
www.atmos-chem-phys.org/acpd/3/1415/

Atmospheric Chemistry and Physics Discussions

The roles of dynamical variability and aerosols in cirrus cloud formation

B. Kärcher[1] **and J. Ström**[2]

[1]Deutsches Zentrum für Luft- und Raumfahrt (DLR), Institut für Physik der Atmosphäre, Oberpfaffenhofen, Germany
[2]Stockholm University, Institute of Applied Environmental Research, Stockholm, Sweden

Received: 5 February 2003 – Accepted: 11 March 2003 – Published: 14 March 2003

Correspondence to: B. Kärcher (bernd.kaercher@dlr.de)

Abstract

The probability of occurrence of ice crystal number densities in young cirrus clouds is examined based on airborne measurements. The observations have been carried out at midlatitudes in both hemispheres at equivalent latitudes ($\sim 52 - 55^{\circ}$ N/S) during the same season (local autumn in 2000). The in situ measurements considered in the present study include temperatures, vertical velocities, and ice crystal concentrations, the latter determined with high precision and accuracy using a counterflow virtual impactor. Most young cirrus clouds typically contain high number densities ($1 - 10\ \mathrm{cm}^{-3}$) of small (diameter $< 20\,\mu$m) ice crystals. This mode dominates the probability distributions in both hemispheres and is shown to be caused by rapid cooling rates associated with updraft speeds in the range $10 - 100\ \mathrm{cm\,s}^{-1}$. A second mode containing larger crystals extends from $\sim 1\ \mathrm{cm}^{-3}$ to low concentrations close to the detection threshold ($\sim 3 \times 10^{-4}\ \mathrm{cm}^{-3}$) and is associated with lower updraft speeds. Results of a statistical analysis provide compelling evidence that the dynamical variability of vertical air motions on the mesoscale is the key factor determining the observed probability distributions of pristine ice crystal concentrations in cirrus. Other factors considered are variations of temperature as well as size, number, and ice nucleation thresholds of the freezing aerosol particles. The variability in vertical velocities is likely caused by atmospheric waves. Inasmuch as gravity waves are widespread, mesoscale variability in vertical velocities can be viewed as a universal feature of young cirrus clouds. Large-scale models that do not account for this subgrid-scale variability yield erroneous predictions of the variability of basic cirrus cloud properties. Climate change may bring about changes in the global distribution of updraft speeds, mean air temperatures, and aerosol properties. As shown in this work, these changes could significantly modify the probability distribution of cirrus ice crystal concentrations. This study emphasizes the key role of vertical velocities and mesoscale variability in vertical velocities in controlling cirrus properties. The results suggest that, in any effort to ascribe cause to trends of cirrus cloud properties, a careful evaluation of dynamical changes in cloud formation

ACPD

3, 1415–1451, 2003

should be done before conclusions regarding the role of other anthropogenic factors, such as changes in aerosol composition, are made.

1. Introduction

It has long been recognized that dynamical processes influence the characteristic, heterogeneous macrostructure of cirrus clouds. Relevant dynamical processes in the upper troposphere and tropopause region include mesoscale gravity waves (e.g. arising from convection or from synoptic-scale weather systems operating over a wide range of scales between a few and many tens of kilometers; lee waves generated downwind of mountain ridges; background air turbulence as a result of shear generation (e.g. near the jet stream); and intrinsic turbulence generated by latent heat and radiative processes within cloud. Turbulence and wave activity often appear as coupled phenomena and cannot easily be separated. Model studies highlighted the complex suite of interactions between radiative, microphysical, and dynamical processes in cirrus clouds (Starr and Cox, 1985; Zhang et al., 1992). Knowledge of dynamical factors influencing both, cirrus cloud macrophysical properties and microphysical structure is required to assess the radiative effects of cirrus and hence their role in climate (Stephens et al., 1990; Quante and Starr, 2002).

Comparatively little emphasis has been put on the role dynamical processes play during the formation of cirrus clouds, although the processes affecting cloud formation may influence the entire life cycle of the cloud. An early field study revealed that ice crystal properties in cirrus clouds are strong functions of the vertical velocity w and temperature T (Heymsfield, 1977). The potential impact of atmospheric waves on the physical properties of young cirrus clouds, in particular on the number concentration n_i of small (diameter below 20 μm) ice crystals, was demonstrated in airborne measurements (Ström et al., 1997). Orographic effects on cirrus were reported in field studies (Heymsfield and Miloshevich, 1993). The importance of mountain waves for the generation of polar stratospheric (ice) clouds in the Arctic is well recognized (Carslaw et al.,

ACPD
3, 1415–1451, 2003

1998).

Most parcel models have used a simplified dynamical setup with constant cooling rates to study the initiation of the ice phase in detail (Lin et al., 2002). One model study pointed out the essential role of scale-dependent vertical wind fields on ice crystal concentration and other cloud parameters (Jensen et al., 1994). Another study investigated the influence of waves on cirrus formed by homogeneous freezing (Lin et al., 1998). A parameterization scheme describing the formation of cirrus clouds was derived from basic physical principles (Kärcher and Lohmann, 2002, 2003), connecting n_i with the variables w and T describing the dynamical cloud forcing, and with parameters of the freezing aerosol particles establishing the microphysical link. Simulations of cirrus clouds in a general circulation model (based on the parameterization) called for the need to better represent subgrid scale variability of vertical motions to predict cloud properties (Lohmann and Kärcher, 2002), a crucial aspect we elucidate further in the present study.

The role aerosol particles from natural and anthropogenic sources play in cirrus cloud formation is not yet adequately understood. The possible aerosol impact on cloud properties is very difficult to quantify. Concerns were raised about potential modifications of cirrus clouds by aircraft particle emissions and contrails (Boucher, 1999; IPCC, 1999). One model study demonstrated that carbonaceous aerosol particles exhausted by aircraft jet engines, when assumed to act as efficient ice nuclei in weak updrafts, could expand cirrus cover and change physical and optical cloud properties (Jensen and Toon, 1997). However, systematic studies aimed at assessing the role of aerosols in cirrus modification that cover a wider range of dynamical forcings – a point we are addressing in more detail in this work – are not available.

In the present study, we gain insight into basic properties and formation mechanisms of upper tropospheric cirrus clouds from examining the probability distributions of measured pristine ice crystal number densities. The aforementioned parameterization is employed to study the relative importance of dynamical factors and properties of the freezing aerosol for cirrus formation. The calculations are mostly based on wind, tem-

ACPD
3, 1415–1451, 2003

perature, and aerosol data gathered during the INCA (Interhemispheric Differences in Cirrus Properties From Anthropogenic Emissions) campaign and are compared with ice crystal concentrations measured simultaneously. We focus on cirrus forming in situ and do not address the generation of cirrus by convective detrainment of cloud condensate.

2. INCA Data

During the INCA experiment, the DLR (Deutsches Zentrum für Luft- und Raumfahrt) research aircraft Falcon was operated out of Punta Arenas, Chile, in the southern hemisphere (SH) campaign and out of Prestwick, Scotland, in the nothern hemisphere (NH) campaign. The campaigns comprised 30 – 40 flight hours each in autumn and employed an identical set of instruments to measure meteorological variables and radiative, chemical, and microphysical properties of aerosol and cirrus cloud particles. Most flight patterns were designed to probe young cirrus clouds and their formation regions in upper cloud layers. This minimizes the influence of ice crystal sedimentation in the data set that could otherwise result in relatively low concentrations of large crystals in cloud layers where freezing is not active. An overview of the INCA experiment and the instruments deployed is available elsewhere (Gayet et al., 2002; Seifert et al., 2003).

2.1. Temperatures and vertical velocities

The Falcon temperature measurments were made with a Rosemount total temperature probe located underneath the nose of the aircraft. Airflow approaching the housing and the sensor in flight generates a dynamical heating due to flow stagnation. This heating must be accounted for using the pressure measurements of the airflow system to obtain the desired static air temperature T, constituting the major source of error in the temperature measurements. The uncertainty of T is better than ± 0.5 K.

The vertical wind component was deduced by substracting the vertical component of

ACPD
3, 1415–1451, 2003

aircraft motion relative to the ground and the vertical component of aircraft motion relative to the surrounding air. The latter is measured with a 5-hole-probe system with a relative precision (random noise) $< 3\,\mathrm{cm\,s^{-1}}$ and a probable bias $\sim 20\,\mathrm{cm\,s^{-1}}$. The bias may be an unknown function of airspeed and air density an hence vary between different flight segments at different altitudes, while being almost constant during straight flight at constant speed. The vertical aircraft speed was determined by differentiation of the measured pressure using the hydrostatic equation. Therefore its absolute accuracy is limited by the equivalency of vertical aircraft motion and horizontal pressure gradients. This leads to typical biases of the order $10\,\mathrm{cm\,s^{-1}}$ (corresponding to an assumed horizontal gradient of 2 kPa per 1000 km). To reduce random noise to levels comparable to that of the airflow measurement, the output was filtered with a cut-off frequency of 0.1 Hz. In summary, a bias error of $\pm 30\,\mathrm{cm\,s^{-1}}$ and a random noise of less than $\pm 5\,\mathrm{cm\,s^{-1}}$ can be assumed. More details of the calibration of the Falcon wind measurement system are discussed elsewhere (Bögel and Baumann, 1991).

The measured magnitude of w depends on the horizontal scale probed by the aircraft. Vertical motions of the order of a few $\mathrm{cm\,s^{-1}}$ may be associated with synoptic scale uplifts (scale 100 km or more). Vertical winds with a few $\mathrm{m\,s^{-1}}$ are associated with isolated convective cells (scale of the order of 1 km). Intermediate mesoscale wave structures with wavelengths λ of several tens of km are associated with velocity amplitudes of several tens of $\mathrm{cm\,s^{-1}}$. The variances of the w distributions ($\sim 25\,\mathrm{cm\,s^{-1}}$, see below) thus indicate the prevalence of mesoscale variability during the cirrus measurements in both campaigns. Note that mesoscale (wave) motion can occasionally lead to updrafts in excess of $1\,\mathrm{m\,s^{-1}}$ and less than $1\,\mathrm{cm\,s^{-1}}$, indicating that a clear distinction between synoptic, mesoscale, and convective forcings cannot always be made.

The limited precision of the w measurements ($\pm 5\,\mathrm{cm\,s^{-1}}$, see above) implies that slow uplifts are not very well represented in the data sets, although they comprise a significant number of measurements. As the w data have been taken at 1 Hz resolution but do not carry information above 0.1 Hz due to filtering, fluctuations of w on scales

ACPD
3, 1415–1451, 2003

below 1.8 km are not resolved, assuming a typical true airspeed of 180 m s^{-1}.

Figure 1 depicts the probability of occurrence of temperature (top) and updraft vertical velocity (bottom) measured during INCA, separated into NH (black distributions) and SH (blue distributions) data sets. The underlying data sets comprise all individual measurements made below 235 K. (This criterion is used to focus on pure ice clouds.) We note that there are no significant differences between the distributions taken inside cloud and the corresponding ones containing all data points. The data sets comprising updraft and downdraft regions are nearly symmetrical (not shown), peaking at -0.5 cm s^{-1} (NH) and -3.9 cm s^{-1} (SH), hence, within the precision of the instrument. This indicates that there is no significant bias in the overall distributions shown in Fig. 1.

The campaign averages of T and w are given in Fig. 1. While mean temperatures are near 225 K in both cases, a few more data points below 215 K exist in the SH data set. The NH data set contains a larger number of updraft speeds above ~ 100 cm s^{-1} than the SH data set, consistent with occasional convective activity observed during the NH campaign, but not in the SH. Note that the statistics becomes very poor for values $w > 160$ cm s^{-1}. There is only a slight interhemispheric difference of 3.2 cm s^{-1} between the mean values.

The green distribution of w shown in Fig. 1 (bottom) is generated from a modified NH data set, where most of the measurements associated with pollution plumes that entered the upper troposphere via rapid vertical transport towards the end of the campaign have been removed. The polluted events were characterized by enhanced concentrations of carbon monoxide (CO) and reactive nitrogen, enhanced levels of turbulence, and increased frequency of occurrence of cumulus clouds. Such events have not been observed in the SH during the campaign. The NH average CO volume mixing ratio in the upper troposphere was near 70 ppb (Baehr et al., 2003). The green distribution was obtained by excluding all data points with CO mixing ratios > 90 ppb. While the distribution below ~ 100 cm s^{-1} is almost unaffected, the impact of convective activity originally seen at higher vertical wind speeds is significantly reduced; the mean

ACPD
3, 1415–1451, 2003

value of w decreases only slightly by 0.4 cm s^{-1}.

In summary, the distributions of w (and T) were remarkably similar in both hemispheres during the INCA campaigns, especially when the influence of convection is removed from the NH measurements. The similarity of the vertical wind distributions may be purely coincidental; based on general circulation patterns, there should be significant differences in updraft speeds and cooling rates between the two hemispheres. In fact, measurement location and timing were chosen to minimize differences in meteorological conditions in order to focus on possible cirrus cloud modification induced by different aerosol properties.

2.2. Aerosol particle size distributions

We present the average aerosol size and number parameters derived from the measurements in Table 1. The parameters refer to multimodal lognormal functions that were used to fit the measured size distributions. The model described in Sect. 3.1 also assumes that the freezing aerosol particles are lognormally distributed and employs these parameters. More details about observations of aerosol particles during INCA are discussed by Minikin et al. (2003).

2.3. Ice crystal concentrations

To generate distribution functions for the number density n_i of cirrus ice crystals, we used all measurements where the counterflow virtual impactor (CVI) counted ice particles (i.e., $n_i > 0$) and where the temperature was below the approximate spontaneous freezing limit of pure water drops ($T < 235$ K). Figure 2 depicts the distribution functions of ice crystal concentrations taken by the CVI as black histograms. The CVI counts the residual particles remaining from evaporating cirrus ice crystals and assumes a one-to-one relation between the residual particle and ice crystal number density (Noone et al, 1988; Ström et al., 1997). This assumption is based on a careful intercomparison of several independent cloud probes deployed during INCA (Gayet et al., 2002; Seifert

ACPD
3, 1415–1451, 2003

et al., 2003). For number densities above $\sim 1\,\mathrm{cm}^{-3}$, the CVI tends to underestimate the ice crystal concentrations. The reason is most likely that at these concentrations, some very small crystals are present with sizes below or close to the lower cut-off of the CVI, which is around 5 μm in diameter.

On average, more ice crystals have been observed in the NH than in the SH, compare the black distributions in Fig. 2. The distributions of n_i taken in both hemispheres exhibit a similar shape, with a broad feature extending from $n_i \simeq 0.1\,\mathrm{cm}^{-3}$ down to the smallest concentrations ($\sim 3 \times 10^{-4}\,\mathrm{cm}^{-3}$, close to the CVI detection limit), and a pronounced primary maximum in the concentration range $0.1 - 10\,\mathrm{cm}^{-3}$. Both distributions also show a secondary maximum at $\sim 0.02\,\mathrm{cm}^{-3}$. The observations of high numbers of relatively small ice crystals in the primary peak regions shown in Fig. 2 is believed to be a robust result (Gayet et al., 2002). In the NH (SH), the broad feature contains 43 % (39 %) and the primary peak region contains 50 % (61 %) of the data, respectively. In the NH data set, 7 % of the measurements indicate very high number densities of up to $200\,\mathrm{cm}^{-3}$.

The SH distribution and the NH distribution cleared of convective episodes are strikingly similar, compare the black SH histogram with the green NH stair steps in Fig. 2. The corresponding mean ice crystal concentrations are virtually identical. Given the fact that the dynamical forcings are nearly identical in both data sets (see Fig. 1), we begin to suspect that the actual properties of the freezing aerosol particles do not strongly affect the number distribution of ice crystals in cirrus. We will discuss this issue further in Sect. 4.

3. Results

3.1. Methodology

We connect the observed values of n_i and w, T, aerosol size distribution parameters, and freezing threshold relative humidities $\mathrm{RHI}_{\mathrm{cr}}$ using a parameterization scheme for

ACPD
3, 1415–1451, 2003

homogeneous and heterogeneous freezing nucleation (Kärcher and Lohmann, 2002, 2003). This scheme has been shown to reproduce initial ice particle concentrations simulated with a numerical parcel model within about a factor of two. The physical processes upon which the parameterization is based are essentially similar to those considered in detailed numerical simulations of the microphysics of ice initiation in cirrus, see Lin et al. (2002) for an overview. The values n_i are calculated using the individual measurements of w and T, not the binned distributions shown in Fig. 1.

In the calculations, we consider freezing of one single, chemically uniform aerosol type. Homogeneous freezing is assumed for the SH data set. Homogeneous freezing thresholds are known functions of T and are of the order 155 % for the mean air temperatures of interest (Koop et al., 2000). Heterogeneous freezing is assumed for the NH data set, with a nominal value $\mathrm{RHI}_{\mathrm{cr}} = 130\,\%$. Both choices for $\mathrm{RHI}_{\mathrm{cr}}$ are motivated by, and consistent with, analyses of relative humidities (Ström et al., 2003; Haag et al., 2003b) measured during INCA (Ovarlez et al., 2002). The freezing aerosol size distribution parameters are noted in Table 1.

It is not known which combinations of w and T can be attributed to cloud formation events. It is therefore not meaningful to study the distribution of n_i for all possible combinations of w and T, as this would lead to a uniform distribution of n_i. Also, not all signatures of small-scale dynamical activity may be captured by the distributions of w employed here. However, it is meaningful to perform a statistical analysis of the measurements: varying one parameter and keeping the others fixed at their average (most probable) values allows to examine separately the sensitivity of the calculated concentration spectrum of ice crystals on the variability of aerosol parameters, temperatures, and updraft speeds.

3.2. SH data

The left column in Fig. 3 shows the results obtained with the SH data set. In Fig. 3a, T was set to the mean value 224.7 K, w was set equal to the mean value 23 $\mathrm{cm\,s^{-1}}$, and aerosol parameters n, D, and σ were varied around average values (see below).

ACPD
3, 1415–1451, 2003

In Fig. 3b, aerosol parameters and w were fixed, the employed distribution function of T is depicted in Fig. 1. In Fig. 3c, aerosol parameters and T were fixed, the employed distribution function of w is depicted in Fig. 1.

Aerosol variability. To produce the green distribution in Fig. 3a, the average aerosol parameters noted in Table 1 have been varied within the ranges $\{0.2n, 2.5n\}$, $\{0.2D, 2.5D\}$, and $\{0.8\sigma, 1.25\sigma\}$ for all modes; 50 000 randomly distributed combinations of the 9 parameters have been generated. With these variations we likely overestimate the actual aerosol variability during INCA.

Figure 3a demonstrates that the variability introduced by rather large changes of the aerosol spectral paramaters produces an extremely narrow spectrum of ice crystal number densities, with a mean value of 0.5 cm^{-3}. This relative insensitivity is expected on the basis of theoretical considerations, if only one type of freezing aerosol is present (Kärcher and Lohmann, 2002, 2003).

Temperature variability. To produce the green distribution in Fig. 3b, 59 444 ice crystal concentrations have been computed based on the observed temperatures. The spectrum of n_i shows some spread in the range 0.2 – 2 cm^{-3}, with a mean value of 0.7 cm^{-3}. To produce the blue distribution, the same calculation has been carried out, but each temperature was lowered by 3 K (consistent with homogeneous freezing thresholds around 155 %) accounting for the fact that the ice-supersaturated regions within which the probed clouds formed were actually colder than the cloud-free environment. As a result, supercooling causes the distribution of n_i to shift slightly towards higher concentrations (mean value 0.9 cm^{-3}). The variance of n_i remains much smaller than observed in both cases.

Updraft variability. To produce the green distribution in Fig. 3c, 31 059 ice crystal concentrations have been computed based on the observed updraft speeds. The spectrum of n_i is much broader than in the other cases, bracketing the range 3×10^{-3} – 40 cm^{-3}, with a mean value of 1 cm^{-3}. In this case, a pronounced peak region develops in the concentration range 0.1 – 5 cm^{-3}, as seen in the observations (top panel in Fig. 2).

ACPD
3, 1415–1451, 2003

Recall that the precision of the vertical velocity measurements is $\pm 5\,\mathrm{cm\,s^{-1}}$. This implies that the low velocity portion of the distribution shown in Fig. 1 is inaccurate in a range where most of the measurements have been taken, while the mid and high velocity ranges are largely unaffected. To account for these effects, the vertical velocities were randomized in the region below $10\,\mathrm{cm\,s^{-1}}$,

$$w \longrightarrow \max\{0.2\,\mathrm{cm\,s^{-1}}, RAN(0,1)\cdot w\}\,,$$

where $0 \le RAN(0,1) \le 1$ denote uniformly distributed random numbers. Note that a lower cut-off has been introduced. Further, random noise was added to the data above $10\,\mathrm{cm\,s^{-1}}$,

$$w \longrightarrow w + RAN(-1,1)\cdot 5\,\mathrm{cm\,s^{-1}}\,,$$

where $-1 \le RAN(-1,1) \le 1$ again denote random numbers.

The result is shown as the blue distribution in Fig. 3c. While the primary peak region and mean crystal number density are only weakly affected by the added noise, the distribution broadens in the low concentration region and develops a secondary maximum, in better agreement with the observations. The ad-hoc cut-off at $0.2\,\mathrm{cm\,s^{-1}}$ produces a relative maximum in the leftmost bin and prevents nucleation of ice with concentrations below about $\sim 3\times10^{-4}\,\mathrm{cm^{-3}}$. The mean value of $1\,\mathrm{cm^{-3}}$ is similar to value inferred from the original data. However, the peak region is not well reproduced by the calculation, compare with the observed spectrum given in Fig. 2 (top).

Recall that not all wave signatures that actually caused freezing may be represented by the distributions of w shown in Fig. 1. Thus it is reasonable to account for the action of gravity waves at intermediate vertical wind speeds by adding a positive component to w with random amplitudes $0 - 20\,\mathrm{cm\,s^{-1}}$ in the range $10 - 80\,\mathrm{cm\,s^{-1}}$

$$w \longrightarrow w + RAN(0,1)\cdot 20\,\mathrm{cm\,s^{-1}}\,.$$

The net effect of the empirical randomization is to increase the mean value of w by $4.1\,\mathrm{cm\,s^{-1}}$ (NH) and $4.3\,\mathrm{cm\,s^{-1}}$ (SH). It should be kept in mind that n_i is a nonlinear

ACPD
3, 1415–1451, 2003

function of w, taking the form $n_i \propto w^k$, with $k = 1, \cdots, 3$ (Kärcher and Lohmann, 2002). Averaging over a wave cycle leads to $n_i > 0$, as ice particles only nucleate when w is positive (in the ascending branch of the wave). This procedure is further motivated by the fact that many mesoscale wave features ($\lambda = 10 - 20$ km) were evident in the vertical wind components in cirrus observed during the First International Satellite Cloud Climatology Project Regional Experiment (FIRE) (Gultepe and Starr, 1995). The associated components of w showed amplitudes up to 20 cm s^{-1}.

The resulting distribution (red stair steps) takes into account empirical corrections accounting for noise and waves and is plotted in Fig. 4 (left) along with the observations (histograms). While the broad feature in the low concentration region is only weakly affected by the added biases, the distribution now nicely reproduces the observed primary peak region caused by a redistribution of data points at concentrations above 0.1 cm^{-3}.

3.3. NH data

The right column in Fig. 3 and the right panel in Fig. 4 show the results of a similar analysis using the NH data set.

Aerosol variability. The baseline aerosol parameters listed in Table 1 have been varied within the same ranges as in the SH case; in addition, we varied the nominal heterogeneous freezing threshold of $RHI_{cr} = 130$ % randomly in the range 120 – 140 %. The result is shown in Fig. 3d as a green distribution, leading to a value of 1 cm^{-3} for the predicted mean ice crystal concentration. Another calculation was performed using the homogeneous freezing thresholds, which is shown as the blue distribution with a mean value of 0.5 cm^{-3}.

The spectrum based on heterogeneous freezing is somewhat more variable and predicts about twice as much ice crystals as the homogeneous case. The higher variability is mainly caused by the imposed lower value of the heterogeneous freezing threshold and its random variations. This is expected, as the sensitivity of n_i to

ACPD
3, 1415–1451, 2003

changes of aerosol parameters increases with decreasing freezing threshold (Kärcher and Lohmann, 2003). When the freezing thresholds are lower, growth rates of pristine ice particles are smaller, resulting in a delayed depletion of supersaturation, allowing more ice particle to be formed.

Temperature variability. To produce the green distribution in Fig. 3e, 50,412 ice crystal concentrations have been computed based on the observed temperatures. The spectrum of n_i shows some spread in the range 0.6 – 6 cm^{-3}, with a mean value of 1.1 cm^{-3}. A similar result, shifted towards lower concentrations with a mean of 0.5 cm^{-3}, is obtained when freezing is assumed to occur homogeneously.

Although we carry out calculations assuming that all aerosol particles trigger freezing around 130 %, we believe that it is unlikely that the high concentrations oberved in the primary peak region in Fig. 3e are caused by such efficient ice nuclei. The number density of such particles is likely to be much smaller than $\sim 1\,cm^{-3}$, except perhaps in the vicinity of in situ sources as for example aging aircraft plumes.

Updraft variability. To produce the green distribution in Fig. 3f, 25,672 ice crystal concentrations have been computed based on the observed updraft speeds. The spectrum of n_i is much broader than in the other cases, bracketing the range 3×10^{-3} – 100 cm^{-3}, with a mean value of 1.8 cm^{-3}. As in the SH case, a pronounced peak region develops around 1 cm^{-3}, consistent with the observations (bottom panel in Fig. 2). Adding noise to the data (blue distribution) as described above significantly improves the agreement with the observations, as it was the case with the SH data set.

Finally, Fig. 4 (right panel) depicts the observed spectrum (histogram) along with a calculated distribution (red stair steps) that has been computed with the mean temperature of 226.2 K, with random noise added to the full spectrum of w, and with random components added to w to empirically account for wave-induced variability. The resulting distribution is similar to the observed one, but the agreement is not as good as in the SH case. Differences are noticeable both at the lowest and the highest concentrations.

ACPD
3, 1415–1451, 2003

3.4. Sources of uncertainties

The calculated NH spectrum depicted in Fig. 4 overestimates the location of the peak region and does not show the observed third mode at very high (10 – 100 cm^{-3}) concentrations (1). The same calculated spectrum decays more rapidly than the observed spectrum at concentrations below 0.01 cm^{-3}, even with the addition of noise to the vertical wind (2). The following factors left unconsidered above could lead to an improvement.

(1) More ice particles are found at very high concentrations as compared to the SH. However, the few events associated with rapid vertical transport that generate the third peak at concentrations above 20 cm^{-3} in the NH data set are not explicitly resolved. (Recall the discussion of Figs. 1 and 2 in Sects. 2.1 and 2.3, respectively.) This averages out the actual behavior seen in the observed spectrum. This argument is supported by means of Fig. 5, where we have repeated the calculations that led to Fig. 4 (right panel) using the modified NH data set where most of the high CO events have been removed. Further, we have used the slightly modified set of aerosol parameters deduced from the reduced data set without high CO measurements, as given in Table 1.

The agreement between observed and modeled distribution improves, especially in the primary peak region. The remaining differences between both are likely caused by the approximate method to account for waves in our model, which is less accurate in the NH case as more small-scale variability was evident during the measurements than in the SH case. It is not possible to infer sources for the variability in vertical velocities from the data, however, wave structures were at times evident in the cloud fields. Likely candidates for waves are orographic forcings induced by mountain ridges in both, NH and SH measurements, perturbations induced by weather systems in the NH measurements, especially during the convective events, and perhaps shear-induced turbulence created near the jet stream. We will study the effects of empirical changes of the vertical velocity spectrum on the distribution of n_i further in Sect. 4.1.

In the parameterization, the sticking probability α of water vapor moleclues impinging

ACPD
3, 1415–1451, 2003

onto the surfaces of growing ice particles (commonly referred to as deposition coefficient) is set equal to 0.5. The sensitivity of n_i on α is small when α varies in the range 0.1 – 1, but increases rapidly below $\alpha = 0.1$ (Lin et al., 2002). It has been argued that very low values of the deposition coefficient, $0.001 < \alpha < 0.1$, could serve as an explanation of the high number densities of ice crystals observed during INCA (Gierens et al., 2003).

To study the effects of small values of α on n_i, the ice crystal distribution (without supercooling and the effect of waves) has been recalculated with $\alpha = 0.05$ (blue stair steps) and $\alpha = 0.2$ (green stair steps). The result for $\alpha = 0.05$ shown in Fig. 6) is not consistent with the SH data (histogram). The peak region is shifted to the right and is significantly broadened, resulting in a mean value of $28\,\mathrm{cm}^{-3}$. Such high values have not been measured with the CVI; the Forward Scattering Spectrometer Probe (FSSP) detected slightly higher concentrations than the CVI, but not to the extent shown by the blue curve. Values $n_i = 100\,\mathrm{cm}^{-3}$ are now predicted with high probabilities of 0.03, but no ice crystals with concentrations above $20\,\mathrm{cm}^{-3}$ have been observed. The low concentration region is shifted to higher values and the secondary peak vanishes, worsening the agreement below $\sim 1\,\mathrm{cm}^{-3}$. For $\alpha = 0.2$, the situation improves at low concentrations, but still the model significantly overestimates the high number density portion of the spectrum. Similar results are obtained in the NH case. Hence, exceptionally low values of α are not supported by the field measurements, consistent with previous findings (Haag et al., 2003a).

(2) The calculations do not account for the fact that homogeneous and heterogeneous freezing may occur simultaneously. Haag et al. (2003b) presented strong evidence that this was the case during the NH measurements by analyzing relative humidity measurements taken during INCA. In the NH, freezing started at 130 %, but the peak humidities measured inside cloud extended to the homogeneous limits, suggesting that ice nuclei contributed to cirrus formation but did not frequently prevent homogeneous freezing from occurring. Kärcher and Lohmann (2003) have emphasized that the competition for available water vapor between ice crystals nucleating from potent

ACPD
3, 1415–1451, 2003

ice nuclei and liquid particles will lead to a suppression of n_i (negative Twomey effect for cirrus clouds) by up to an order of magnitude in cases where all available ice nuclei are frozen but freezing of liquid particles is not yet initiated. How much crystal concentrations are suppressed depends on the temperature, the freezing threshold of ice nuclei, and, most importantly, on the vertical wind speed and number concentrations of ice nuclei relative to the liquid particles.

Based on these findings, it is highly conceivable that a refined formulation for freezing in the calculation could improve the agreement with the NH observations by further broadening the low concentration part of the spectrum and, at the same time, by shifting the peak region more to the left. A better understanding of the freezing processes prevalent during INCA is required before this conjecture can be tested; this is not within the scope of the present work, but will be investigated in the future.

4. Discussion and Summary

We have demonstrated that the variability in vertical motion alone can explain the key features of observed distribution of n_i, emphasizing the important role of mesoscale waves. While synoptic-scale updrafts affect the low concentration regime ($< 0.1\,\mathrm{cm}^{-3}$), mesoscale variability explains the occurrence of the peak region at intermediate concentrations ($0.1 - 10\,\mathrm{cm}^{-3}$), and convection may cause another maximum in the high concentration regime ($> 10\,\mathrm{cm}^{-3}$). Mesoscale waves, however, can also contribute to the low and high concentration regions, depending on the exact phase of the waves at and above the freezing threshold (Lin et al., 1998). Below we study the impact of changed dynamical forcing and aerosol properties on the distribution of n_i and the vertical motion variability as computed by large-scale models.

ACPD
3, 1415–1451, 2003

4.1. Dynamical variability

How does the spectrum of ice crystal concentration changes when the spectrum of vertical winds changes in a future climate? It is not known how vertical motions will change in the future. Even for the current atmosphere, a global climatology of vertical air motion is not available. However, we may estimate potential changes of the distribution of n_i by prescribing different vertical wind distributions in our model.

Figure 7 (top panel) depicts the NH vertical wind distribution already discussed in Sect. 2.1 as black stair steps. The blue distribution (labeled "less waves") results from dividing these values by 1.5. The frequency of occurrence of velocities $> 30\,\mathrm{cm\,s^{-1}}$ is reduced, while lower winds speeds are more likely to occur. The green distribution (labeled "more waves") is obtained by multiplying each value of w of the black distribution by 1.5. Here, the frequency of occurrence of velocities $> 30\,\mathrm{cm\,s^{-1}}$ is enhanced while lower winds speeds occur with reduced probability.

Figure 7 (bottom panel) depicts the resulting distributions of n_i, using the same color code. These calculations consider the addition of noise and wave-driven variability to the original vertical velocities, as described in Sect. 3. Compared to the baseline case (mean n_i value of $2.3\,\mathrm{cm^{-3}}$ from the model), the mean concentrations vary by factors 0.5–2 when the wave-driven forcing is reduced or enhanced by a factor of 1.5. We note that a decrease of the average air temperature by 3 K would lead to roughly comparable changes of the distribution of n_i (compare with Fig. 3b). In particular, from Fig. 7 we infer that the probability to find concentrations of $\sim 0.05\,\mathrm{cm^{-3}}$ nearly doubles and the probability to find values of $10\,\mathrm{cm^{-3}}$ rises almost by a factor of 8.

Summary. At midlatitudes during INCA, the spectrum of w was largely governed by mesoscale variability, with sufficient potential to preferentially activate the homogeneous freezing mode. Enhancing or suppressing this variability may significantly alter the distribution of ice crystal concentrations in young cirrus clouds. As gravity waves appear to be widespread also in other atmospheric regions, such as the tropical upper troposphere and tropopause region (Karoly et al., 1996) or the Arctic polar lower strato-

ACPD
3, 1415–1451, 2003

sphere (Dörnbrack and Leutbecher, 2001), it is highly likely that our findings also apply to other cases, including tropical cirrus and polar stratospheric clouds. Our results clearly call for the need to better understand the sources and characteristics of gravity waves near the tropopause as a prerequisite to study their impact on cirrus formation in more detail.

4.2. Vertical motion variability in large-scale models

It is interesting to deliniate implications of our results for simulations of cirrus clouds with large-scale atmospheric models. Specifically, we describe the upper tropospheric vertical wind fields taken from the European Centre for Medium-Range Weather Forecasts (ECMWF) global model and the ECMWF-model Hamburg version (ECHAM), and discuss resulting probability distributions of n_i obtained with our approach. Noise and wave-induced variability is not added to the global wind fields.

The first set of global calculations were based on operational ECMWF wind fields (within 150 – 350 hPa) with $\sim$ 40 km horizontal resolution; smaller-scale gravity waves, non-hydrostatic waves, and deep convection are not explicitly resolved. To date, cirrus clouds are not simulated interactively in the ECMWF forecast system, as in most other global models. The second set of global model results was based on ECHAM large-scale wind fields (within 175 – 275 hPa) with $\sim$ 300 km horizontal resolution; again, smaller-scale dynamical forcings are not explicitly resolved. However, in another set of ECHAM wind fields, a mesoscale component proportional to the turbulent kinetic energy is added to the large-scale mean value of the vertical velocity to approximately account for subgrid-scale variability of vertical air motion. The latter wind fields have been employed to simulate cirrus clouds interactively in ECHAM. More details of the ECMWF and ECHAM simulations are discussed in Haag et al. (2003b).

Can current large-scale models reliably predict cirrus cloud properties? The answer is no, because such models do usually not consider the subgrid-scale variability of vertical air motion in the calculation of cirrus cloud properties. Figure 8 (left) shows the green distribution of w from the ECMWF model. Given the steep decrease of the

ACPD
3, 1415–1451, 2003

distribution as compared to the cloud-scale observations and the low mean vertical velocity of 1.3 cm s^{-1}, the synoptic-scale updrafts result in an ice crystal concentration spectrum and a mean n_i value in striking disagreement with both, the observations and our model, see Fig. 8 (right).

Figure 8 (left) shows the ECHAM results using the large-scale winds only (red) and with the mesoscale components added to the large-scale winds (blue). The ice crystal distribution based on large-scale winds is worse than the ECMWF result (red distribution in the right panel), as the mean large-scale vertical velocity from ECHAM is smaller than the ECMWF mean. This is mainly caused by the much coarser horizontal and vertical resolution of the ECHAM model.

However, the ECHAM results improve when mesoscale variability is accounted for (blue distributions in Fig. 8). The distribution of w now extends into the convective regime, but still severly underestimates the intermediate mesoscale regime and overemphasizes the lowest wind speeds. Compared with the large-scale only case (red distributions), the ice crystal distribution is shifted towards higher concentrations. While this approach leads to quite realistic distributions of relative humidity in ice-supersaturated regions (Haag et al., 2003b), the vertical velocity does not exhibit the same fine scale structure as indicated by observations and is therefore unable to reproduce distributions of n_i as those measured during INCA (Lohmann et al, 2003).

In judging about the present ECHAM results including subgrid-scale variability, we note that the simulated ice crystal concentrations represent mean values averaged over a model grid box. These averages cannot be directly compared to the observations (or, equivalently, to our model results); the same holds for the ECMWF results. However, taken as grid box means, the mean number density of 0.7 cm^{-3} predicted by ECHAM is a reasonable value.

Summary. It is highly desirable to develop a prognostic parameterization for the subgrid-scale variability of vertical air motion caused by waves on the mesoscale. Such a parameterization, ideally combined with prognostic schemes for the ice cloud number density (Lohmann and Kärcher, 2002; Wilson and Ballard, 1999) and perhaps fractional

ACPD
3, 1415–1451, 2003

cirrus cover in the spirit of Tompkins (2002), could be coupled to the parameterization of cirrus cloud formation developed recently (Kärcher and Lohmann, 2002, 2003).

4.3. Indirect aerosol effect on cirrus

At the end of Sect. 2.3, we saw the possibility emerging that details of the freezing processes have little impact on certain cirrus cloud properties. The subsequent analysis provided further evidence for a limited indirect aerosol effect on the distribution of ice crystals in young cirrus clouds, because the general shape of the distributions of n_i is strongly controlled by the distribution of vertical velocities.

To gain additional insight, we have used the average SH aerosol parameters (including the freezing threshold) in conjunction with NH vertical winds and vice versa to calculate distributions of n_i. The results are shown in Fig. 9, where the best estimate model results (repeated from Fig. 4 and now plotted as black stair steps) are contrasted with the results obtained by exchanging the interhemispheric aerosol size distribution and freezing properties (plotted as blue distributions) for the NH (top panel) and the SH (bottom panel).

It is interesting to note that the general shape of the curves does not depend on the assumption whether freezing occurs purely homogeneously or purely heterogeneously. The mean value of n_i roughly varies within a factor of two between both cases. Keeping the cloud ice water content fixed, halving or doubling n_i (as induced by the aerosol changes) will increase or decrease the mean number diameter of the ice crystals by a factor of $2^{1/3} = 1.26$.

The aerosol-induced changes in the distributions of n_i between each of the two scenarios are mainly caused by the different freezing thresholds ($\sim 130\,\%$ versus $\sim 155\,\%$, compare Figs. 3d and 3e). In the primary peak region, they are comparable to those induced by the perturbed vertical winds as shown in Fig. 7 and are less dramatic in the region around the secondary peak. However, as noted above, inclusion of competition between different types of freezing nuclei may more strongly modify the low concentration part of the n_i distribution.

ACPD
3, 1415–1451, 2003

Our findings are useful in outlining two potential consequences of aerosol-induced cirrus modifications.

First, it is possible that ice nuclei exert a substantial influence on the properties of optically thin cirrus clouds with low ice crystal number densities generated in weak updrafts. This argument has been raised earlier for the special subset of subvisible cirrus clouds (Kärcher, 2002). The impact of heterogeneous freezing diminishes with increasing updraft speed (or increasing n_i), because the number of efficient ice nuclei present in the upper troposphere will be limited and will stay below the total number of available aerosol particles. In optically thicker cirrus clouds, ice nuclei will create the first ice crystals which grow to the largest sizes. These crystals will preferentially sediment to lower altitudes. The associated vertical redistribution of ice water mass and ice nuclei may lead to enhanced dehydration of upper cloud levels near the tropopause and to enhanced seeding of ice in mixed phase clouds at lower levels.

Second, the spatial extent and frequency of occurrence of cirrus may increase with decreasing freezing thresholds RHI_{cr}, as the atmosphere contains more weakly ice supersaturated regions than regions with high supersaturations near the homogeneous limit. How much the areal ratio between highly and more weakly supersaturated regions changes depends on details of the atmospheric dynamics (Kärcher and Haag, 2003) and is difficult to predict. On the other hand, even moderate changes in the dynamical forcing may likewise affect the spatial and temporal cirrus coverage.

Summary. As we neither know how upper tropospheric abundances of ice nuclei nor how vertical wind and temperature fields change in a future climate, it is difficult to estimate the relative importance of the indirect aerosol effect and changes in the dynamical forcing patterns on cirrus clouds. In any case, we reiterate that homogeneous or heterogeneous freezing alone would largely be consistent with the observations, provided the dynamical forcing is adequately taken into account. We have shown that cirrus formation is at least as, and probably more, sensitive to changes in dynamical forcing patterns as to changes in the aerosol size and number. More significant changes may occur when mixtures of liquid particles and efficient ice nuclei are present. This very

ACPD
3, 1415–1451, 2003

likely leads to a partial redistribution of ice crystal concentrations, not to a substantial change of the distribution functions of n_i; however, we did not yet achieve sufficient understanding of the actual freezing mechanisms in cirrus clouds to reach a definite conclusion.

The consequences of these proposed modifications for the cloud life cycle and its radiative properties are not clear at this point and need to be assessed in the future. Differencing between natural and anthropogenic causes of possible cirrus cloud changes in a future climate or trends in cirrus cloud cover will require a very careful and detailed analysis of underlying processes.

5. Conclusions

The conclusions of this study are as follows:

1. The general shape of the distribution of ice crystal concentrations in young cirrus clouds observed at midlatitudes during INCA consists of a predominant primary peak at concentrations 0.1 – 10 cm^{-3}, and a less pronounced, secondary peak at $\sim 0.02\,\mathrm{cm}^{-3}$ embedded in a broad feature extending to concentrations of $\sim 3 \times 10^{-4}\,\mathrm{cm}^{-3}$. Another peak at concentrations 10 – 100 $\mathrm{cm\,s}^{-1}$ appeared in NH measurements, but not in the SH data set.

2. Mesoscale variability in updraft velocities in combination with pure homogeneous freezing processes accounts for most of the observed variance in number densities of ice crystals. Mean ice particle concentrations may decrease when efficient ice nuclei compete with liquid particles during cirrus cloud formation. While the assumption of pure heterogeneous freezing would also be consistent with the present observations, number densities of upper tropospheric ice nuclei are likely to be too low to account for a substantial fraction of ice crystals observed in the primary peak region.

3. Mesoscale variability in vertical velocities in the range 10 – 100 $\mathrm{cm\,s}^{-1}$ caused by atmospheric waves accounts for much of the observed high number densities (0.1 – 10 cm^{-3}) of ice crystals in young cirrus. Strong convective forcing can produce even

ACPD
3, 1415–1451, 2003

higher ice particle concentrations. The impact of heterogeneous freezing processes in these concentration regions is minimal.

4. Large-scale or wave-driven variations in vertical velocities below $10\,\mathrm{cm\,s^{-1}}$ account for much of the observed low number densities ($< 0.1\,\mathrm{cm^{-3}}$) of ice crystals in young cirrus. The impact of heterogeneous freezing processes in this concentration region is potentially large.

5. It is difficult to assess the relative importance of the indirect aerosol effect and changes in the dynamical forcing patterns on cirrus clouds in a future climate. Both factors could alter cirrus cloud properties by similar amounts, but the current knowledge about mesoscale updraft variability (especially induced by gravity waves) and freezing mechanisms in cirrus clouds is very limited and prevents definite conclusions to be drawn.

6. There is an urgent need to improve the representation of vertical air motions in large-scale models. Improving the representation of subgrid-scale variability in updraft speeds, or cooling rates, in atmospheric models is an essential prerequisite to predicting cirrus clouds globally and to study their role in climate change scenarios.

Acknowledgements. We are grateful to R. Baumann, W. Haag, and A. Minikin for help with the INCA data base, and to U. Lohmann for providing output from simulations carried out with the ECHAM general circulation model. Thanks also go to A. Dörnbrack and D. Fahey for helpful discussions. This research was conducted within the projects "Particles in the Upper Troposphere and Lower Stratosphere and Their Role in the Climate System" (PARTS) and "Interhemispheric Differences in Cirrus Properties From Anthropogenic Emissions" (INCA), both funded by the European Commission. It contributes to the project "Particles and Cirrus Clouds" (PAZI) supported by the Helmholtz-Gemeinschaft Deutscher Forschungszentren (HGF). One of us (BK) acknowledges the hospitality of the staff at the Meteorological Institute at Stockholm University (MISU) during a scientific stay and thanks K. Noone and D. Nilsson for stimulating discussions.

References

Baehr, J., Schlager, H., Ziereis, H., Stock, P., van Velthoven, P., Busen, R., Ström, J., and Schumann, U.: Aircraft observations of NO, NO_y, CO and O_3 in the middle and upper tro-

posphere from 60° N to 60° S – Interhemispheric differences at midlatitudes, Geophys. Res. Lett., submitted, 2003. 1421
Bögel, W. and Baumann, R.: Test and calibration of the DLR Falcon wind measuring system by maneuvers, J. Atmos. Oceanic Technol., 8, 5–18, 1991. 1420
Boucher, O.: Influence of air traffic on cirrus occurrence, Nature, 397, 30–31, 1999. 1418
Carslaw, K. S., Wirth, M., Tsias, A., Luo, B. P., Dörnbrack, A., Leutbecher, M., Volkert, H., Renger, W., Bacmeister, J. T., Reimer, E., and Peter, Th.: Increased stratospheric ozone depletion due to mountain-induced atmospheric waves, Nature, 391, 675–678, 1998. 1417
Dörnbrack, A. and Leutbecher, M.: Relevance of mountain waves for the formation of polar stratospheric clouds over Scandinavia: A 20 year climatology, J. Geophys. Res., 106, 1583–1593, 2001. 1433
Gayet, J.-F., Auriol, F., Minikin, A., Ström, J., Seifert, M., Krejci, R., Petzold, A., Febvre, G., and Schumann, U.: Quantitative measurement of the microphysical and optical properties of cirrus clouds with four different in-situ probes: Evidence of small ice crystals, Geophys. Res. Lett., 29, 24, 2230, doi:10.1029/2001GL014342, 2002. 1419, 1422, 1423
Gierens, K., Monier, M., and Gayet, J.-F.: The deposition coefficient and its role for cirrus clouds, J. Geophys. Res., 108, D2, 4069, doi:10.1029/2001JD001558, 2003. 1430
Gultepe, I. and Starr, D. O'C.: Dynamical structure and turbulence in cirrus clouds: Aircraft observations during FIRE, J. Atmos. Sci., 52, 4159–4182, 1995. 1427
Haag, W., Kärcher, B., Schaefers, S., Stetzer, O., Möhler, O., Schurath, U., Krämer, M., and Schiller, C.: Numerical simulations of homogeneous freezing processes in the aerosol chamber AIDA, Atmos. Chem. Phys., 3, 195–210, 2003a. 1430
Haag, W., Kärcher, B., Ström, J., Minikin, A., Lohmann, U., Ovarlez, J., and Stohl, A.: Freezing thresholds and cirrus cloud formation mechanisms inferred from in situ measurements of relative humidity, Atmos. Chem. Phys., to be submitted, 2003b. 1424, 1430, 1433, 1434
Heymsfield, A. J.: Precipitation development in stratiform ice clouds: A microphysical and dynamical study, J. Atmos. Sci., 34, 367–381, 1977. 1417
Heymsfield, A. J. and Miloshevich, L. M.: Homogeneous ice nucleation and supercooled liquid water in orographic wave clouds, J. Atmos. Sci., 50, 2335–2353, 1993. 1417
Intergovernmental Panel on Climate Change (IPCC): Aviation and the Global Atmosphere, Special Report,Cambridge Univ. Press, New York, 65–120, 1999. 1418
Jensen, E. J., Toon, O. B., Westphal, D. L., Kinne, S., and Heymsfield, A. J.: Microphysical modeling of cirrus, 2. Sensitivity studies, J. Geophys. Res., 99, 10443–10454, 1994. 1418

ACPD
3, 1415–1451, 2003

Jensen, E. J. and Toon, O. B.: The potential importance of soot particles from aircraft exhaust on cirrus clouds, Geophys. Res. Lett., 24, 249–252, 1997. 1418
Kärcher, B.: Properties of subvisible cirrus clouds formed by homogeneous freezing, Atmos. Chem. Phys., 2, 161–170, 2002. 1436
Kärcher, B. and Lohmann, U.: A parameterization of cirrus cloud formation: Homogeneous freezing including effects of aerosol size, J. Geophys. Res., 107, D23, 4698, doi:10.1029/2001JD001429, 2002. 1418, 1424, 1425, 1427, 1435
Kärcher, B. and Lohmann, U.: A parameterization of cirrus cloud formation: Heterogeneous freezing, J. Geophys. Res., 108, doi:10.1029/2002JD003220, in press, 2003. 1418, 1424, 1425, 1428, 1430, 1435
Kärcher, B. and Haag, W.: Factors controlling relative humidity, Atmos. Chem. Phys. Discuss., to be submitted, 2003. 1436
Karoly, D. J., Rolf, G. L., and Reeder, M. J.: Gravity wave activity associated with tropical convection detected in TOGA-COARE sounding data, Geophys. Res. Lett., 23, 261–264, 1996. 1432
Koop, Th., Luo, B. P., Tsias, A., and Peter, Th.: Water activity as the determinant for homogeneous ice nucleation in aqueous solutions, Nature, 406, 611–614, 2000. 1424
Lin, H., Noone, K. J., Ström, J., and Heymsfield, A. J.: Dynamical influences on cirrus cloud formation processes, J. Atmos. Sci., 55, 1940–1949, 1998. 1418, 1431
Lin, R.-F., Starr D. O'C., DeMott, P. J., Cotton, R., Sassen, K., Jensen, E., Kärcher, B., and Liu, X.: Cirrus parcel model comparison project phase 1: The critical components to simulate cirrus initiation explicity, J. Atmos. Sci., 59, 2305–2329, 2002. 1418, 1424, 1430
Lohmann, U. and Kärcher, B.: First interactive simulations of cirrus clouds formed by homogeneous freezing in the ECHAM GCM, J. Geophys. Res., 107, D10, 4105, doi:10.1029/2001JD000767, 2002. 1418, 1434
Lohmann, U., Kärcher, B., and Timmreck, C.: Impact of the Mt. Pinatubo eruption on cirrus clouds formed by homogeneous freezing in the ECHAM GCM, J. Geophys. Res., 108, revised manuscript under review, 2003. 1434
Minikin, A., Petzold, A., Ström, J., Krejci, R., Seifert, M., van Velthoven, P., Schlager, H., and Schumann, U.: Aircraft observations of the upper tropospheric fine particle aerosol in the northern and southern hemispheres at midlatitudes, Geophys. Res. Lett., 30, 10.1029/2002GL016458, in press, 2003. 1422
Noone, K., Ogren, J. A., Heintzenberg, J., Charlson, R. J., and Covert, D. S.: Design and cali-

bration of a counterflow virtual impactor for sampling of atmospheric fog and cloud droplets, Aerosol Sci. Technol., 8, 235–244, 1988. 1422

Ovarlez, J., Gayet, J.-F., Gierens, K., Ström, J., Ovarlez, H., Auriol, F., Busen, R., and Schumann, U.: Water vapour measurements inside cirrus clouds in Northern and Southern hemispheres during INCA, Geophys. Res. Lett., 29 (16), 1813, doi:10.1029/2001GL014440, 2002. 1424

Quante, M., and Starr, D. O'C.: Dynamical processes in cirrus clouds, in: *Cirrus*, Lynch, D.K., Sassen, K., Starr, D.O'C., Stevens, G. (Eds.), Oxford Univ. Press, New York, 346–374, 2002. 1417

Seifert, M., Ström, J., Krejci, R., Minikin, A., Petzold, A., Gayet, J.-F., Schumann, U., and Ovarlez, J.: In-situ observations of aerosol particles remaining from evaporated cirrus crystals: Comparing clean and polluted cases, Atmos. Chem. Phys., 3, under review, 2003. 1419, 1422

Starr, D. O'C. and Cox, S. K.: Cirrus clouds, Part II: Numerical experiments on the formation and maintenance of cirrus, J. Atmos. Sci., 42, 2682–2694, 1985. 1417

Stephens, G. L., Tsay, S. C., Stackhouse, P. W., and Flatau, P. J.: The relevance of the microphysical and radiative properties of cirrus clouds to climate and climatic feedback, J. Atmos. Sci., 47, 1742–1753, 1990. 1417

Ström, J., Strauss, B., Anderson, T., Schröder, F., Heintzenberg, J., and Wendling, P.: In situ observations of the microphysical properties of young cirrus clouds, J. Atmos. Sci., 54, 2542–2553, 1997. 1417, 1422

Ström, J. et al.: Cirrus cloud occurrence as a function of ambient relative humidity: A comparison of observations from the Southern and Northern hemisphere midlatitudes obtained during the INCA experiment, Atmos. Chem. Phys. Discuss., to be submitted, 2003. 1424

Tompkins, A.: A prognostic parameterization for the subgrid-scale variability of water vapor and clouds in large-scale models and its use to diagnose cloud cover, J. Atmos. Sci., 59, 1917–1942, 2002. 1435

Wilson, D. R. and Ballard, S. P.: A microphysically based precipitation scheme for the UK Meteorological Office Unified Model, Q. J. R. Meteorol. Soc., 125, 1607–1636, 1999. 1434

Zhang, Y., Laube, M., and Raschke, E.: Evolution of stratiform cirrus simulated in a lifting layer, Contr. Atmos. Phys., 65, 23–34, 1992. 1417

Table 1. Size distribution parameters of aerosol particles measured during INCA. The measurements are fitted to superimposed lognormal modes. Given are the campaign averages of the total number n, mean number diameter D, and geometrical width σ for each individual mode from the northern (NH) and southern hemisphere (SH) measurements; NH (no convection) is based on the NH data set cleared of pollution events associated with convection

SH				
n [cm^{-3}]	110	40	–	0.06
D [μm]	0.021	0.084	–	0.7
σ	1.4	1.8	–	1.7
NH				
n [cm^{-3}]	300	70	20	0.07
D [μm]	0.018	0.05	0.14	0.7
σ	1.49	1.6	1.5	1.8
NH (no convection)				
n [cm^{-3}]	200	50	40	0.07
D [μm]	0.014	0.03	0.1	0.7
σ	1.4	1.5	1.65	1.7

ACPD
3, 1415–1451, 2003

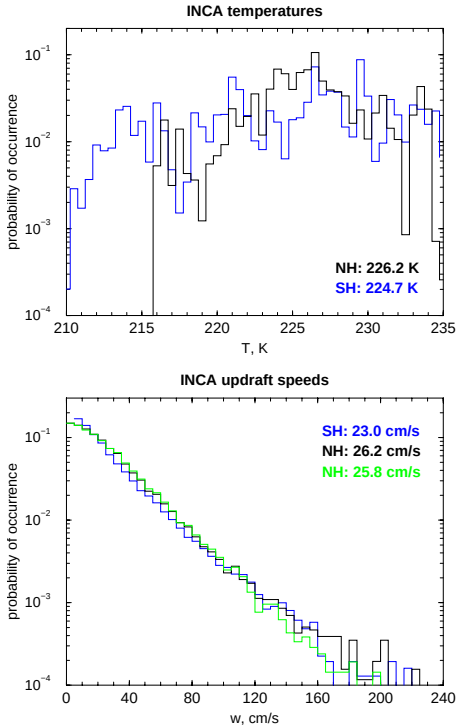

Fig. 1. Distributions of static air temperature T (top) and upwind vertical velocity w (bottom) derived from the Prestwick data set (NH, black distributions) and the Punta Arenas data set (SH, blue distributions). Mean values are indicated. The data sets represent all values measured below 235 K. To produce the green distribution of w, we have removed all NH measurements associated with rapid vertical transport and convective influence (see text for details). Temperatures and vertical wind speeds were binned into 0.5 K and 5 cm s^{-1} intervals, respectively.

ACPD
3, 1415–1451, 2003

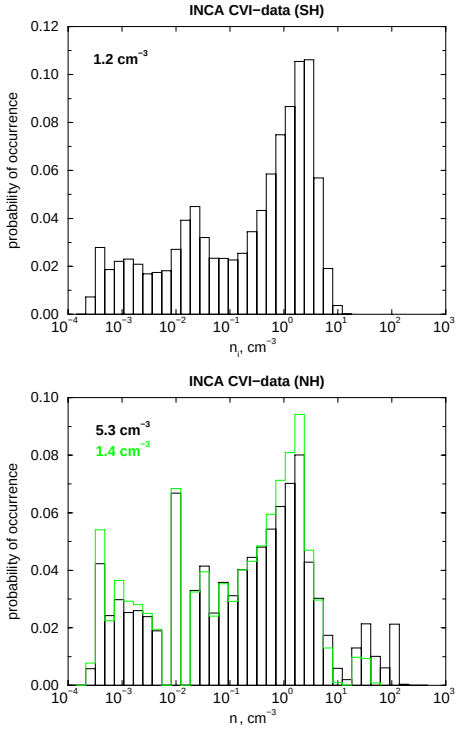

Fig. 2. Distributions (black histograms) of number densities n_i of ice crystals for the Punta Arenas data set (SH, top) and the Prestwick data set (NH, bottom). The underlying data sets represent measurements inside cloud below 235 K. Measurements in strongly polluted air masses affected by rapid vertical transport and convection are removed in the green distribution shown in the bottom panel. Mean values of n_i are indicated. A logarithmic concentration grid was used and number densities were binned into constant $\Delta n_i/n_i = 0.4$ intervals (sucessive bin center values n_i increase by a factor of 1.5).

ACPD
3, 1415–1451, 2003

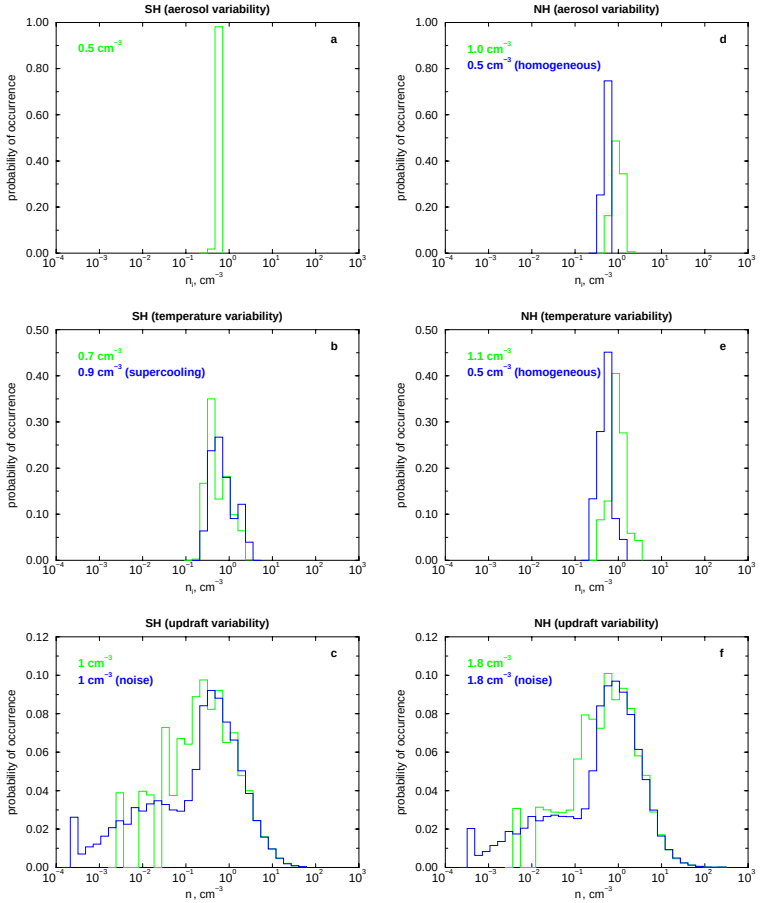

Fig. 3. Calculated distribution functions of ice particle number densities for the SH (a–c) and the NH (d–f). Mean values of n_i are indicated. See text for details.

ACPD
3, 1415–1451, 2003

Dynamical variability, aerosols, and the formation of cirrus clouds

B. Kärcher and J. Ström

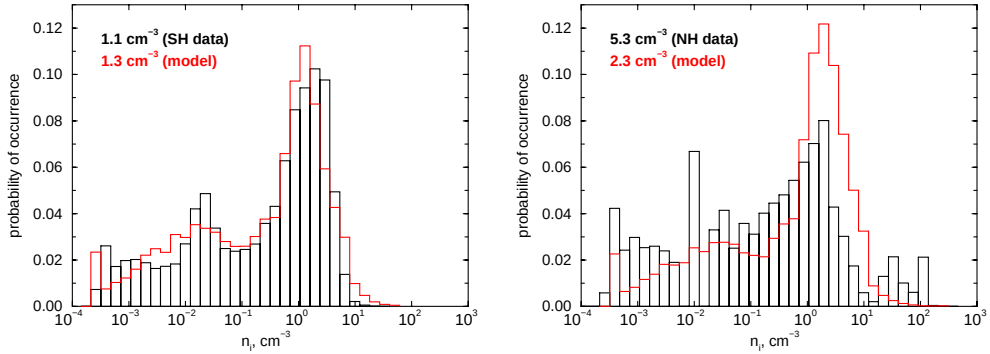

Fig. 4. Calculated (red stair steps) and observed (black histograms, taken from Fig. 2) distribution functions of ice particle number densities for the SH (left) and the NH (right). Mean values of n_i are indicated. The modeled distributions account for mesoscale wave-driven variability (in the range 10 – 100 cm s^{-1}) and noise (±5 cm s^{-1}) in the vertical velocity data and are calculated at average temperatures using average aerosol parameters. See text for details.

ACPD
3, 1415–1451, 2003

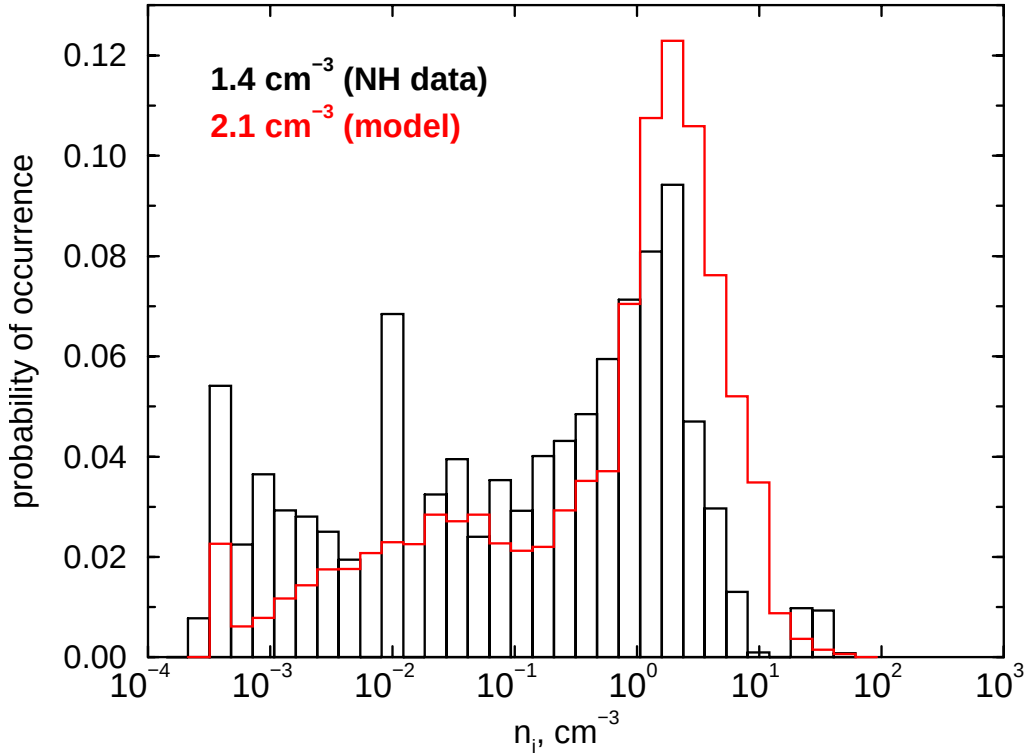

Fig. 5. Same as Fig. 2 (right panel), but using n_i and w measurements approximately cleared of convective influence.

ACPD
3, 1415–1451, 2003

Dynamical variability, aerosols, and the formation of cirrus clouds

B. Kärcher and J. Ström

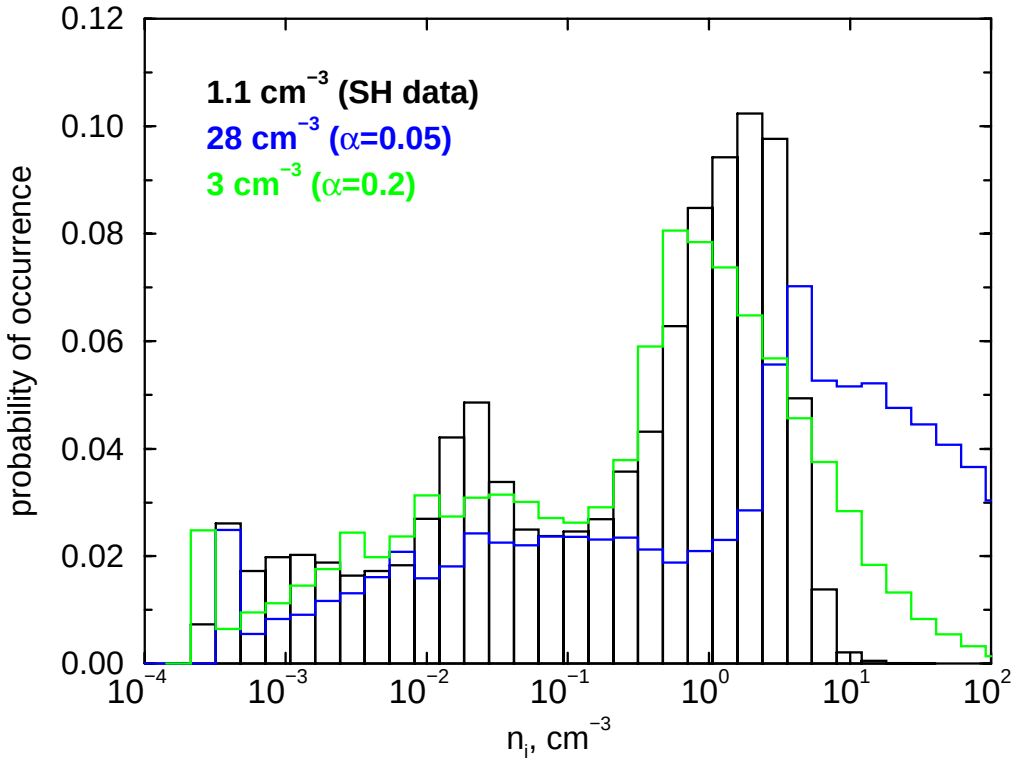

Fig. 6. Observed distribution of n_i in the SH (black histogram) taken from Fig. 2 and spectra calculated with a value for the deposition coefficient α of H_2O molecules on ice lowered by a factor of 10 (blue stair steps) and 2.5 (green stair steps). This calculation does not take into account supercooling and wave-induced variability, which would shift the blue and green distributions to higher concentrations.

ACPD
3, 1415–1451, 2003

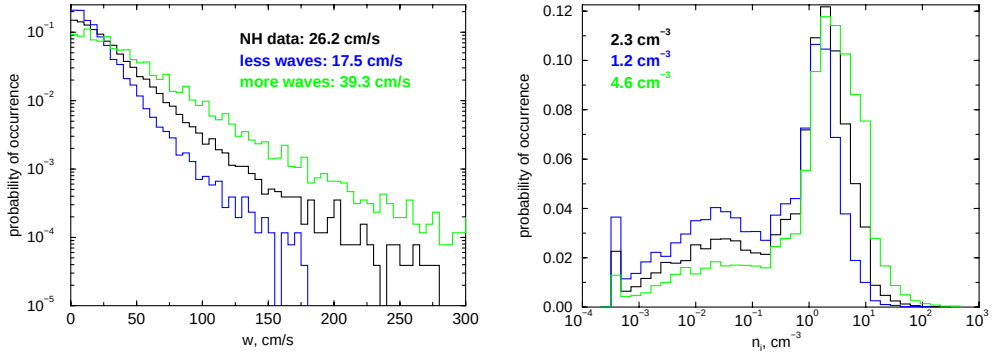

Fig. 7. Distributions of updraft speeds (left panel) from the NH data set (black), and from modified NH data sets with more wave activity (green) and less wave activity (green); the original NH updraft sppeds have been multiplied and divided by a factor of 1.5, respectively. The distributions of n_i obtained from calculations are shown in the right panel. Noise and wave-driven variability was added to all updraft speeds (not shown) to calculate the distributions of n_i.

ACPD

3, 1415–1451, 2003

Dynamical variability, aerosols, and the formation of cirrus clouds

B. Kärcher and J. Ström

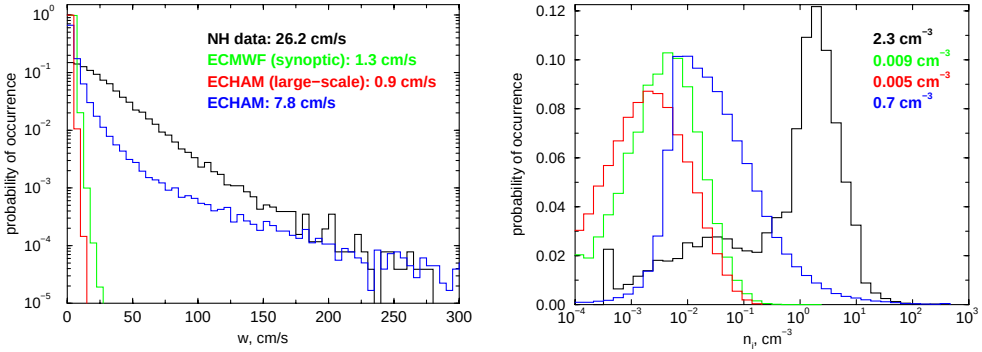

Fig. 8. Distributions of updraft speeds (left panel) from the NH data set (black), from upper tropospheric synoptic-scale winds caluclated by the ECMWF weather forecast model (green), from upper tropospheric large-scale winds caluclated by the ECHAM general circulation model (red), and from corresponding ECHAM simulations where subgrid-scale fluctuations are added to the large-scale vertical wind to approximately account for mesoscale variability (blue). The distributions of n_i obtained from calculations are shown in the right panel. No additional artificial noise or wave-driven variability was added to calculate the distributions of n_i.

ACPD
3, 1415–1451, 2003

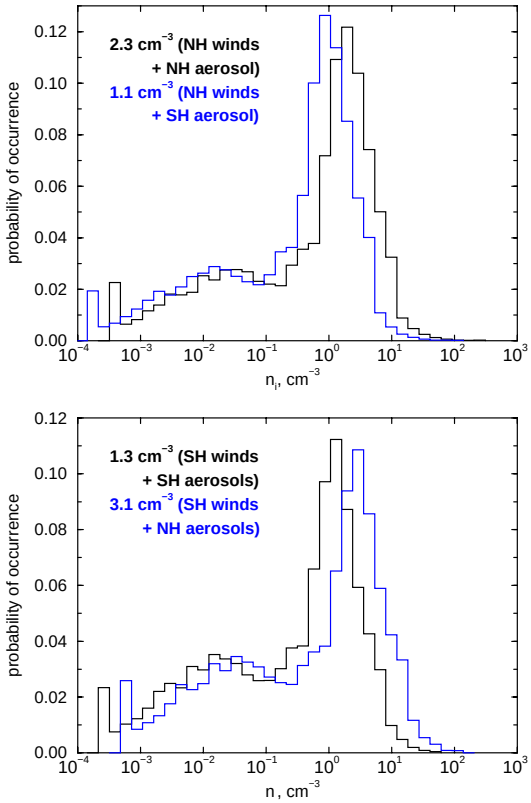

Fig. 9. Calculated distribution functions of ice particle number densities using the NH wind data (top panel) and the SH wind data (bottom panel). The blue distributions use the respective aerosol parameters given in Tab. 1 and are repeated from Fig. 4 (shown there in red). The green distributions use exchanged aerosol parameters. Mean values of n_i are indicated.

ACPD
3, 1415–1451, 2003